Hybrid effect of fiber mesh and short fibers on the biaxial bending behavior of TRC

Dong LI[a], Yining DING[a,*], Qing WANG[a], Yongchao ZHANG[a], Cecilia AZEVEDO[b], Yulin ZHANG[b]

[a] *State Key Laboratory of Coastal and Offshore Engineering, Dalian University of Technology, Dalian 116024, China,* [b]*Centre of Mathematics, University of Minho, Braga 4700-052, Portugal*

Abstract: The textile mesh reinforced concrete/mortar (TRC/M) has been studied in recent years. However, the current testing methods are focused on simply supported member under uniaxial bending, which are inadequate for analyzing of the biaxial tensioned fiber mesh and also incapable to reveal the biaxial behavior of the TRC panel. Besides, the fibers can be damaged by the alkali ambient of concrete. In order to overcome the inadequacy, a series experiment of two-way panels is carried out. The methodology used here consists of the experiment and the analysis of the experimental data, including the evaluation of alkali resistance, the biaxial bending capacity and toughness of two-way slabs. The suitable fibers are selected based on alkali resistance, and the effect of fiber meshes on the biaxial bending capacity of the two-way TRC slabs is studied. Through addressing the disadvantages of brittle fiber mesh reinforced TRC compared to conventional reinforced concrete panel, a significant increment of the ductility of TRC panel with steel fibers is achieved. Following the analysis of the experimental data, it can be concluded that the conventional steel mesh with reinforcement ratio of 0.2% can be replaced by the combined use of glass/basalt fiber mesh and steel fibers.

Keywords: composite materials; reinforcement; durability-related properties; slabs & plates; load & loading; toughness

* Corresponding author. Tel.: +86 411 84709756.
E-mail address: ynding@hotmail.com (Y. Ding).

Notation			
TRC	textile reinforced concrete	TRM	textile reinforced mortar
PC	plain concrete	RC	conventional steel mesh reinforced concrete
BTRC	textile reinforced concrete with basalt fiber	HSBTRC	hybrid use of 50kg/m^3 macro steel fiber and basalt fiber mesh reinforced concrete
GTRC	textile reinforced concrete with AR glass fiber		
F_1	first-peak load	HSGTRC	hybrid use of 50kg/m^3 macro steel fiber and AR glass fiber mesh reinforced concrete
F_2	second-peak load		
F_u	ultimate load	l	span length
F_{500}	load at deflection of l/500	Q_{500}	energy absorption in deflection from 0 to l/500
F_{250}	load at deflection of l/250	Q_{250}	energy absorption in deflection from 0 to l/250
F_{100}	load at deflection of l/100	Q_{100}	energy absorption in deflection from 0 to l/100
F_{50}	load at deflection of l/50	Q_{50}	energy absorption in deflection from 0 to l/50

1. Introduction

Series of previous investigations have reported that the mechanical properties of the concrete can be increased noticeably by the addition of discrete short fibers such as steel fiber, basalt fiber and plastic fiber etc (Alhozaimy *et al*., 1996; Ding *et al*., 2014; Enfedaque *et al*., 2010; Jain and Singh, 2013; Lee *et al*., 2016; Li and Xu, 2009; Lim *et al*., 2011; Ros *et al*., 2016; Sim *et al*., 2005; Singh, 2016; Song *et al*., 2004; Wang *et al*., 2009; You *et al*., 2017; Zollo, 1997). Due to the high load-bearing capacities, the performance of the textile mesh reinforced concrete or mortar (TRC/M) has been much concerned by the investigators in recent years (Bernat *et al*., 2013; Chira *et al*., 2016; Gopinath *et al*., 2016; Larrinaga *et al*., 2014; Papanicolaou *et al*., 2007; Shams *et al*., 2014a; Shams *et al*., 2014b; Triantafillou *et al*., 2006; Zargaran *et al*., 2017). Shams *et al*. (2014a; 2014b) evaluated the flexural behavior of two sides simply supported TRC panels, and presented an analytical model to calculate the bending behavior of the one-way TRC slab. Chira *et al*. (2016) studied the flexural properties of a newly developed TRC façade panel, and Zargaran *et al*. (2017) verified the effect of the parameters of the fiber mesh, the reinforcement ratio and the thickness of the specimen on the

bending performance of TRC composites. But, the above mentioned investigations (Chira *et al*., 2016; Shams *et al*., 2014a; Shams *et al*., 2014b; Zargaran *et al*., 2017) was focused on the uni-axial flexural properties of TRC member using static determinate testing system (such as two sides simply supported beam or panel). Bernat *et al*. (2013) investigated the performance of the masonry wall strengthened by the TRM under eccentric compressive loading. Larrinaga *et al*. (2014) verified the uni-axial tensile behavior of the TRM. However, the strong biaxial load-bearing capacity of fiber mesh is still experimentally poor explored. In addition, it is well known that glass fiber, basalt fiber and concrete are all brittle materials. Hence, the incorporation of brittle fiber mesh into brittle concrete/mortar may enhance the strength of TRC/M, but it is incapable to reduce brittleness of the TRC/M member and to prevent catastrophic brittle failure by several mechanisms.

Compared to the conventional steel mesh reinforcement, the basalt/glass fiber mesh may show strong corrosion resistance and excellent biaxial tensile strength. The TRC structural elements can be used as facades (see Fig.1), roofs, panels, permanent formwork elements, tanks and precast elements, like manhole covers for the drainage and cover plate for the urban underground pipelines (Brameshuber, 2006). The concrete matrix shows a strong alkaline ambient, the pH value of the concrete can be over 12 (Mehta, 2006). The prerequisite for the constructive application of various fiber mesh in the infrastructure consists mainly of the following three points: 1) alkaline resistance of fiber mesh in the concrete matrix; 2) the positive effect of fiber mesh on the mechanical properties of concrete, especially on the biaxial tension behavior, and 3) the similar toughness and ductile failure pattern of TRC member compared to conventional steel mesh reinforced RC panel under bending.

Fig.1 TRC facades

In this study, the accelerated alkali resistance test was adopted to verify the chemical corrosion of the medium-alkali glass fiber (C-glass fiber), alkali resistance glass fiber (AR glass fiber) and the basalt fiber. Although some similar investigations have been made in the previous studies (Liu *et al*., 2013; Purnell *et al*., 2000; Rybin *et al*., 2013; Wei *et al*., 2010), but our focus was given on selecting the suitable fiber mesh to be used as the reinforcement of the cementitious materials. The two-way slab test was used to evaluate the bi-axial flexural property of the TRC, the test involves a 600×600×100 mm plate, simply supported on four sides by a rigid metallic frame, and the centre point load applied through a contact surface of 100 x 100 mm (European Federation of Producers and Applications of Specialist Products for Structures, 1996). Additionally, in order to enhance the toughness of the TRC and to replace the conventional steel mesh, the macro steel fiber was adopted, the hybrid effect of the combined use of fiber mesh and macro steel fiber was investigated.

2. Experiments

2.1 Materials

The basic mix proportion was illustrated in Table 1. The cement was ordinary Portland cement (P·O 42.5R); the fine aggregates were quartz sand with the particle size 0-2 mm. The 28 d compression strength of the fine grained concrete was 51.2MPa. Fig.2 demonstrated the basalt fiber used in the test, the fiber mesh (Fig.2 (b)) was manufactured by the corresponding fiber filaments (Fig.2 (a)). The fiber filaments were used for the alkali resistance, and the fiber meshes were used in the concrete slab as reinforcement. There were two types of glass fibers: C-glass fiber (ZrO_2 content

0%) and AR glass fiber (ZrO_2 content 16.7%) used for the alkali resistance test. The 65/35BG macro steel fiber (fiber length 35 mm, aspect ratio 65, tensile strength 1345 N/mm^2) was used as shown in Fig.3. The steel mesh was made by the hot-rolled plain bars with the diameter of 6.5 mm, the mesh size was 150 × 150 mm and the reinforcement ratio was 0.2%. This ratio is often used for members like roofs, facades, floors and manhole cover, etc.

Table 1 Mix proportion of the fine grained concrete

Cement (kg/m^3)	Water (kg/m^3)	Sand(kg/m^3)		Super plasticizer (kg/m^3)
		0-1 mm	1-2 mm	
600	210	360	840	7.2

Fig.2 Basalt fibers: (a) basalt fiber filament; (b) basalt fiber mesh

Fig.3 Macro steel fiber

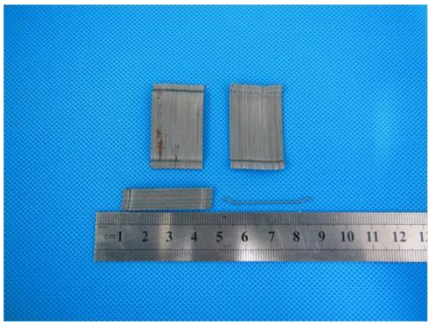

2.2 Alkali resistance test

The concrete matrix shows a strong alkaline ambient, the pH value of the concrete ranges from 12.5 to 13.5 (Mehta, 2006). The accelerated alkali resistance test was carried out based on Ref. (Hou *et al.*, 2007). The fiber filaments were treated in 5% NaOH solution with the constant temperature of 80℃, and the sustained time varied from 0 to 24 h. After the alkaline treatment, the samples were washed by distilled water and dried.

The scanning electron microscope (SEM) was adopted to characterize the surface morphologies of the original fibers and those after the alkaline treatment of 24 h in NaOH solution. The energy dispersive spectroscopy (EDS) was introduced to analyze the significant chemical modification, especially the change of Si element of the fiber filaments.

2.3 Two-way slab test

In order to evaluate the bi-axial bending behavior and the energy absorption of fiber mesh reinforced concrete, the two-way slab test recommended by the EFNARC was adopted (European Federation of Producers and Applications of Specialist Products for Structures, 1996). Similar to the steel mesh, the fiber mesh also showed strong bi-axial tension behavior. The two-way slab was considered to sufficiently reflect the influence of fiber mesh on the mechanical property of cementitious material, especially the fiber mesh effect on the bi-axial bending behavior of mortar/concrete slab.

In this experiment, the dimension of the slabs was 600×600×100 mm, the fiber meshes were arranged at 30 mm from the bottom of the slab. After demoulding, the slabs were placed in curing room immediately before testing. A rigid metallic frame was introduced to simply support the slab on its four edges. A central load was applied through a 100×100 mm precast stiffness bearer (see Fig.4). The deformation rate of the central point was about 1.5 mm/min.

Fig.4 Set-up for bending slab test

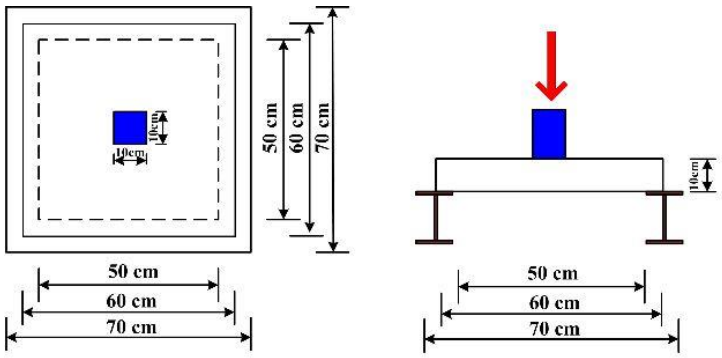

Compared to the conventional two sides simply supported beam test, there are some advantages of four edges simply supported slab as follows: 1) the effect of fiber mesh on the bi-axial bending capacity of the two-way TRC slabs can be better analyzed; 2) the four edges simply supported TRC slab is a three times statically indeterminate structure and allows both inner force redistribution and stress redistribution, hence the loading behavior and failure pattern of TRC related to the inner force redistribution could be evaluated more exactly, whereas the two sides simply supported conventional beam/panel is a static determinate structure, only stress redistribution occurs and no inner force redistribution can take place during the loading process.

3 Test results and discussions

3.1 Alkaline resistance

The prerequisite for the investigation of the mechanical behavior and practical application is the alkaline resistance of the fiber mesh. In order to choose the suitable fiber mesh for the further study on the load bearing capacity of TRC slab, the different filaments are treated in the alkali solution for 24 hours. After the accelerated testing of the alkaline resistance, the corrosion-damaged surfaces of C-glass fiber, AR glass fiber and basalt fiber were compared with the corresponding original fibers without alkali treatment and analyzed using SEM. Fig. 5, Fig. 6 and Fig. 7 show the comparison of surface analysis of different fibers before and after alkali treatment in the 2 mol/L of NaOH solution.

Fig.5 SEM analysis of the C-glass fiber surface: (a) original fiber, (b) after 24 h alkaline treatment

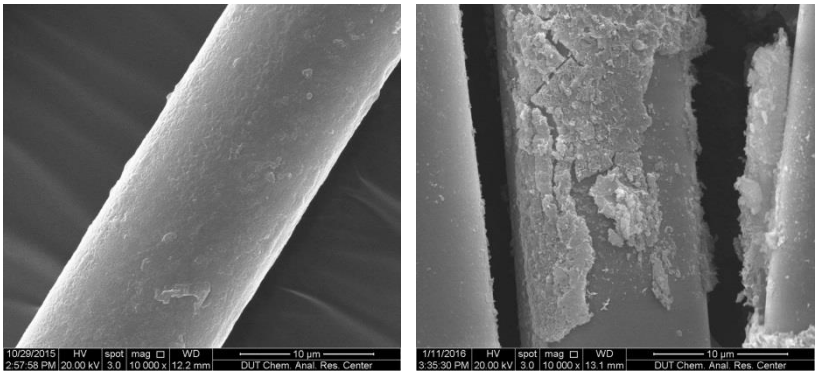

The C-glass fiber has relatively smooth surface relief before alkali attack. Small single surface defects can be found under large magnification (10000 times) as shown in Fig. 5(a). The strong corrosive damage on the surface of the fibers can be observed (see Fig. 5(b)), and for samples immersed into alkali solution for 24 hours, the corrosion shell is peeled off, and the effective diameter of the fiber is reduced clearly. So, such kind of C-glass fiber is not suitable as reinforcement for cement/concrete member, hence it is not selected to the further investigation on the mechanical property of TRM member.

Fig.6 SEM analysis of the AR glass fiber surface: (a) original fiber, (b) after 24 h alkaline treatment

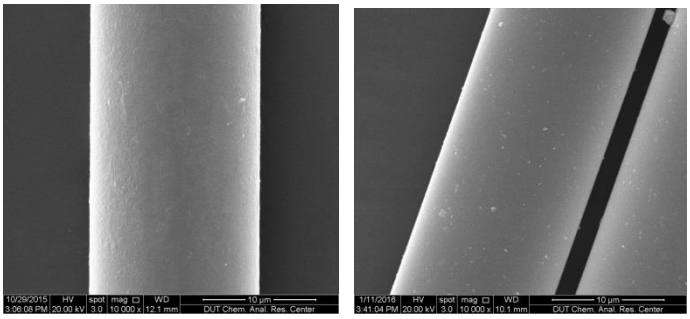

The AR glass fiber has very smooth surface relief even under large magnification (10000 times) as shown in Fig.6 (a). The obviously corrosive damage is not observed on the surface of the fiber after 24h alkaline treatment, as shown in Fig.6 (b).

Fig.7 SEM analysis of the basalt fiber surface: (a) original basalt fiber, (b) basalt fiber after 24 h alkaline treatment

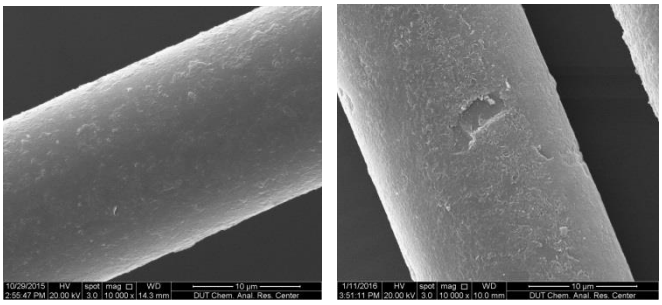

Similar to the C-glass fiber, small single surface defects can also be detected on the basalt fiber (Fig.7 (a)). After 24 h alkaline treatment, only pit areas on the surface of the fiber can be observed (see Fig.7 (b)), and the effective diameter of the fiber will not be affected by the pit areas obviously.

From Figs.5-7, it can be seen that:

- Before the alkaline treatment, the surface of the C-glass fiber, the AR glass fiber and the basalt fiber are very smooth, although some points of the fiber display surface defect which may probably be caused by the abrasion during the manufacturing (Fig.5 (a) and Fig.7 (a)).
- After 24 h alkaline treatment, the formation of a brittle shell was found on the C-glass fiber and basalt fiber filament surface (see Fig. 5 (b) and Fig. 7 (b)). This shell was formed with a certain thickness around the filament and was partially peeled off in some areas. Although the chemical composition of the fibers is different, both fibers react in the similar way. The underlying fiber surface appeared smooth and uncorroded. This was in agreement with observations made by other investigators (Liu *et al*., 2013; Rybin *et al*., 2013; Wei *et al*., 2010), while the surface of the AR glass fiber is still very smooth, and demonstrates good alkali resistance (Fig.6 (b)).

The changes in the composition of the different fibers were investigated by EDS analysis. Integrity and representativeness of the morphological features of the corrosion shell for each sample were taken into consideration in order to choose the suitable filaments for further investigation on the

mechanical behavior. The comparison of Si element of C-glass fiber, AR glass fiber and basalt fiber were given in Table 2.

Table 2 Changes of Si element before and after NaOH treatment (wt %) of different fibers

Element	Si		
	C-glass fiber	AR glass fiber	basalt fiber
Original fiber	43.5	30.2	28.7
After 24 h treatment	31.3	33.8	24.2

From Table 2, it can be seen that compared to the original fiber before alkaline treatment, the Si concentration of the surfaces of C-glass fiber and basalt fiber decreased by about 28% and 16% respectively, whereas the Si contents of AR glass fiber increased by about 12%.

The C-glass fiber seems to deteriorate the performance under severe alkali conditions. The major reason is that the main framework of the glass fiber is the —Si—O— bond, and in the alkaline environment such as NaOH solution, the —Si—O— bond will be broken by the hydroxyl ions (Friedrich *et al*., 2000; Scheffler *et al*., 2009), then the original structure of the fiber is destroyed, the reaction products drop off from the surface and dissolve in the solution. The effective diameter of the fiber reduces noticeably; hence the mechanical properties of the fibers may be decreased significantly.

For the AR glass fiber, the reason for the good alkaline resistance may attribute to the Na_2O-SiO_2-ZrO_2system, which is more chemically stable in alkaline solution (Bentur and Mindess, 2007).

For the basalt fiber, there is only mild damage on the fiber surfaces, the alkali resistance is much better than that of the C-glass fiber. The reasons may ascribe to the T_iO_2 contained in the basalt fiber.

3.2 Flexural properties of two-way TRC slabs

The C-glass fiber mesh was not taken into account for the two-way slab test, because the C-glass fiber showed relatively poor alkali resistance, and was not suitable to be used as the reinforcement of concrete. Only the AR glass fiber mesh and the basalt fiber mesh were adopted as reinforcement for the TRC slab. The different fiber reinforcements of slabs are illustrated in Table 3.

Table.3 Summary of six types of specimens

Types	Basalt fiber mesh	AR glass fiber mesh	Macro steel fiber (kg/m^3)	Steel mesh
PC	—	—	0	—
BTRC	√	—	0	—
GTRC	—	√	0	—
RC	—	—	0	√
HSBTRC	√	—	50	—
HSGTRC	—	√	50	—

Notes: √ means that this kind of reinforced material is added to the slab; — means that this kind of reinforced material is not added into the slab.

Based on the previous investigations (Ding and Kusterle, 1999), the crack patterns of four edges simply supported TRC slab subjected to centre point loading could be postulated in Fig.8.

Fig.8 Cracks pattern of TRC slab

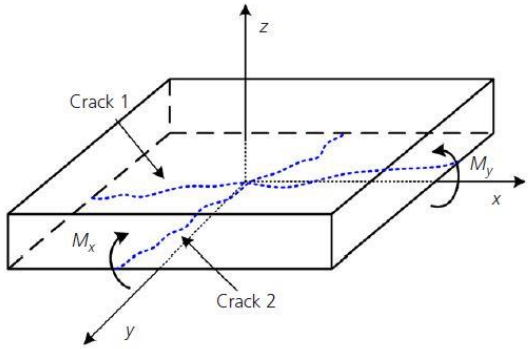

Fig.9 shows the load–deformation curve of the basalt fiber mesh reinforced concrete (BTRC) slab.

Fig.9 Load-deflection curve for BTRC slab

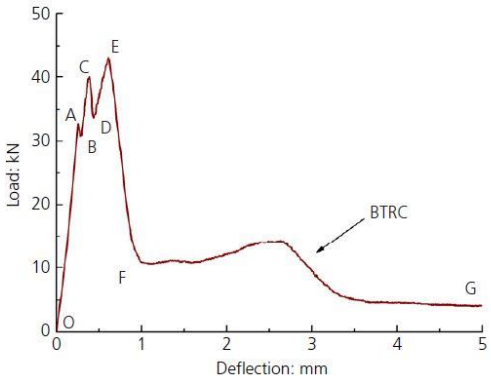

Under central concentrated load, the load-deflection curve of the four edges simply supported square BTRC slab can be divided into three stages (Fig.9):

Stage I (Pre-cracking stage OA): with the increasing of external central loading, the bending moments in two directions M_x and M_y (Fig.8) increase. Before the concrete cracks, the TRC panel behaves more or less elastically. When M_x (or M_y) increases to M_{crx} (e.g. the cracking moment about x-axis), the tensile strain of the concrete of the panel bottom may reach the ultimate tensile strain, the panel achieves the critical state (I_a: the first peak load F_1) and the crack is impending, the corresponding cracking moment can be called as M_{crx} (or M_y), the first structural crack occurs in the weakest section, and the weakest section is distributed randomly in the bottom of the TRC panel. In the Stage I, the deflection increases slowly.

Stage II (Post-cracking stage ABCDE): crossing the first turning point A, TRC panel goes into Stage II (TRC member in the cracking stage). The load drops slightly at point B, if the first concrete crack (e.g. crack 1 in Fig.8) occurs. As the basalt fiber mesh crossing the first crack (assuming: crack1) takes up the tension released by concrete, a clear increase in the tensile stress of fiber mesh may occur. At the same time, the inner force redistributes to another direction (from M_x to M_y) occurs, and the load continues to increase (BC). With the increasing of the loading in part BC of the stage II: the crack 1 near the x-axis develops continually and the stiffness of panel declines gradually, both the inner force redistribution in the other direction and stress redistribution may occur continually.

When M_y increases to M_{cry} (e.g. the cracking moment about y-axis), the new crack 2 takes place near y-axis; When the crack 1 and crack 2 develop and extend fast through the bottom, the load drops again (part CD). After point D, the whole bi-axial tensile forces are carried by the fiber mesh. A significant increment in the tensile stress of fiber mesh in two directions may occur. The load-bearing capacity of the cracked TRC panel may be enhanced further (part DE), and this stage ends with the point E (the ultimate load F_u) as the fiber mesh reaches the ultimate tensile strength.

Stage III (Post-peak stage): Crossing the peak loading (point E/the ultimate load F_u), TRC panel goes into the failure stage. Some bi-axial stressed fiber meshes are broken down suddenly due mainly to the brittle behavior of basalt/glass fibers, and the load bearing capacity of the two-way TRC slab declines significantly (part EF): for point F at the deflection about 1mm, the load bearing capacity declines from 43.1kN up to 10.8kN, it was a decreasing ratio of about 75%. The basalt fiber mesh reinforced concrete panel indicates a strong brittle failure pattern, and it is not suitable for the construction application.

After point F (part FG): the rest of bi-axial tensioned fiber meshes are broken down gradually and the residual load bearing capacity between 1 mm (l/500) to 5 mm (l/100) is in a very low loading level. The cracks (crack 1 and crack 2) in two directions widen significantly, extend along the section height and finally propagate through the whole panel.

Fig.10 shows the comparison of the load–deflection curves of plain concrete (PC) slab, AR glass fiber mesh reinforced concrete (GTRC) slab, BTRC slab and RC slab. The comparison of the first-peak load (F_1), the second-peak load (F_2) and the ultimate load (F_u) is shown in Fig.11.

Fig.10 Comparison of load-deflection curves of PC, BTRC, GTRC and RC slabs

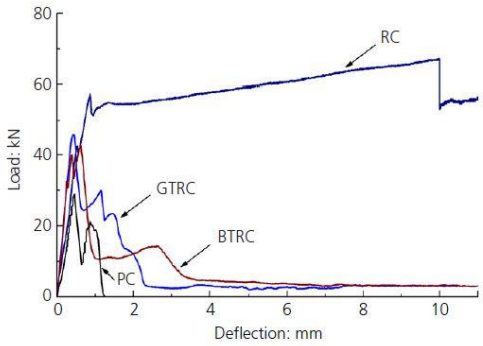

Fig.11 Comparison of the loads of PC, BTRC and GTRC slabs

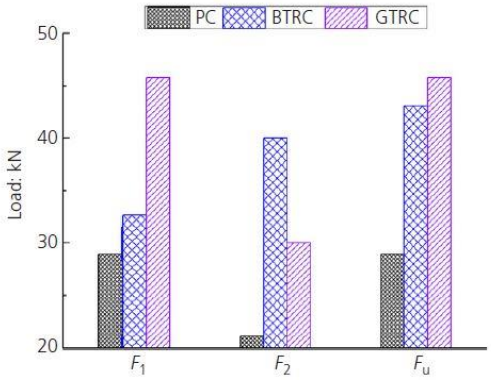

From Fig.10 and Fig.11, it can be seen that:

i) The first-peak loads F_1 of PC slab, BTRC slab and GTRC slab are 28.9kN, 32.7kN and 45.8kN, respectively. Compared to the PC slab, F_1 of the BTRC slab and the GTRC slab increase by about 13% and 58%, respectively.

ii) The second-peak loads F_2 of PC slab, BTRC slab and GTRC slab are 21.1kN, 40.0kN and 30.0kN, respectively. Compared to the PC slab, F_2 of the BTRC slab and the GTRC slab increase by about 90% and 43%, respectively.

iii) The ultimate load of PC slab, BTRC slab and GTRC slab are 28.9kN, 43.1kN and 45.8kN, respectively. Compared to the PC slab, F_u of the BTRC slab and the GTRC slab increase by about 49% and 58%, respectively.

iv) After F_u, both the BTRC slab and the GTRC slab demonstrate low post-peak behavior and the load bearing capacity declines abruptly, after the deflection of 5 mm, the residual loads are reduced to about 3.3kN and 4.1kN, respectively. Compared to F_u, the residual loads of the BTRC slab and the GTRC slab decrease by about 90% and 93%, respectively.

From the observations above, we get that the addition of the fiber mesh may show very positive biaxial effect on the redistribution ability of inner force of the TRC slabs and can enhance the ultimate load F_u of the slab, but the brittle failure pattern of the slab doesn't change obviously. Compared to the ductile failure pattern of conventional RC slab, both basalt and glass fiber mesh

reinforced slab with clear brittle failure pattern are incapable for replacing of steel mesh, and hence unsuitable for the constructive application.

In order to improve the ductility of the TRC slab, the macro steel fibers are added into the TRC slab. Fig.12 shows the comparison of the load–deflection curves of hybrid use of 50 kg/m^3 macro steel fiber reinforced concrete and basalt fiber mesh (HSBTRC) slab, RC slab and BTRC slab. The comparison of the load bearing capacity of BTRC, RC and HSBTRC slabs at different deflections are shown in Table 4.

Fig.12 Comparison of load-deflection curves of BTRC, RC and HSBTRC slabs

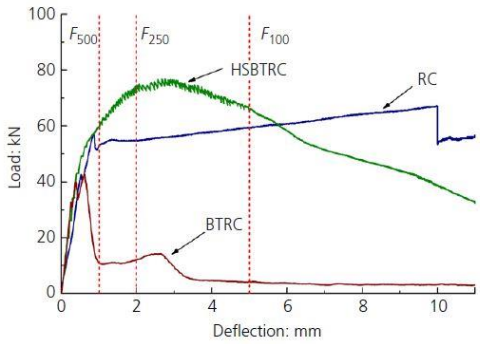

Table4 Comparison of the load bearing capacity

Types	F_u/ kN	δ_u/mm	Load at different deflection / kN			
			F_{500}	F_{250}	F_{100}	F_{50}
BTRC	43.1	0.6	11.1	12.1	4.1	3.2
RC	66.9	9.7	52.8	54.8	59.5	53.1
HSBTRC	76.9	2.8	59.0	73.1	65.5	38.5

Note: F_u means the ultimate load; δ_u means the deflection corresponding to the F_u; F_a (a=500, 250, 100, 50) means the load at the deflections of l/a, l is the span length.

From Fig.12 and Table 4, it can be seen that:

i) The F_u of the HSBTRC slab and the RC slab are 76.9kN and 66.9kN, respectively. Compared to the RC slab, the F_u of the HSBTRC slab increases by about 11%.

ii) The deflection of the BTRC slab and the HSBTRC slab corresponding to the ultimate load F_u are 0.6 mm and 2.8 mm, respectively. Compared to the BTRC slab, the δ_u of the

HSBTRC slab increases by about 366%.The ability of plastic redistribution of inner force is enhanced strongly by the hybrid use of basalt fiber mesh and steel fibers.

iii) The F_{500} of the HSBTRC slab and the RC slab are 59.0kN and 52.8kN, respectively. Compared to the RC slab, the F_{500} of the HSBTRC slab increases by about 12%.

iv) The F_{250} of the HSBTRC slab and the RC slab are 73.1kN and 54.8kN, respectively. Compared to the RC slab, F_{250} of the HSBTRC slab increases by about 33%.

v) The F_{100} of the HSBTRC slab and the RC slab are 65.5kN and 59.5kN, respectively. Compared to the RC slab, F_{100} of the HSBTRC slab increases by about 10%.

vi) The F_{50} of the HSBTRC slab and the RC slab are 38.5kN and 53.1kN, respectively. Compared to the RC slab, F_{50} of the HSBTRC slab decreases by about 27%.

vii) The load-deflection curve of the HSBTRC slab is higher than that of the conventional RC slab over the deflection from 0 to 5 mm.

From the discussion above, it can be summarized that the combined use of basalt fiber mesh and macro steel fiber can improve the flexural load bearing capacity, the toughness of the TRC slab and the ability of plastic redistribution of inner force significantly.

Fig.13 shows the comparison of the load–deflection curves of hybrid use of 50 kg/m^3 steel fiber and AR glass fiber mesh reinforced concrete (HSGTRC) slab, RC slab and GTRC slab. The comparison of the load bearing capacity of GTRC, RC and HSGTRC slabs are shown in Table 5.

Fig.13 Comparison of load-deflection curves of GTRC, RC and HSGTRC slabs

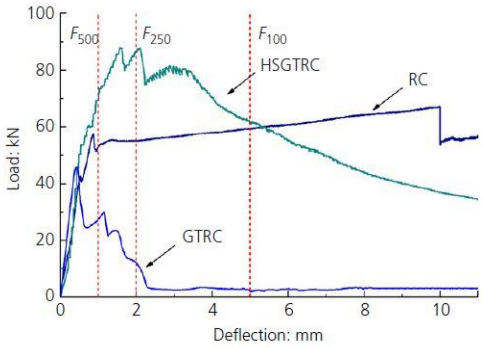

Table 5 Comparison of the load bearing capacity

Types	F_u/kN	δ_u/mm	Load at different deflection /kN			
			F_{500}	F_{250}	F_{100}	F_{50}
GTRC	45.8	0.4	24.6	23.0	3.3	2.9
RC	66.9	9.7	52.8	54.8	59.5	53.1
HSGTRC	88.0	2.1	69.6	86.6	61.3	37.0

From Fig.13 and Table 5, it can be seen that:

i) The ultimate load F_u of HSGTRC slab is 88.0kN. Compared to the RC slab, F_u of the HSGTRC slab increases by about 32%.

ii) The deflection of the GTRC slab and the HSGTRC slab corresponding to F_u are 0.4 mm and 2.1 mm, respectively. Compared to the GTRC slab, the δ_u of the HSGTRC slab increases by about 425%.

iii) The F_{500} of the HSGTRC slab and the RC slab is 69.6kN and 52.8kN, respectively. Compared to the RC slab, F_{500} of the HSGTRC slab increases by about 32%.

iv) The F_{250} of the HSGTRC slab is 86.6kN. Compared to the RC slab, the F_{250} of the HSGTRC slab increases by about 58%.

v) The F_{100} of the HSGTRC slab is 61.3kN. Compared to the RC slab, the F_{100} of the HSGTRC slab increases by about 3%.

vi) The F_{50} of the HSGTRC slab and the RC slab are 37.0kN and 53.1kN respectively. Compared to the RC slab, the F_{50} of the HSGTRC slab decreases by about 30%.

vii) The load-deflection curves of the HSGTRC slab is above the conventional RC slab over the deflection from 0 to 5 mm.

From the discussion above, it can be concluded that the combined use of AR glass fiber mesh and 50kg/m^{3}macro steel fiber can increase the post-peak load bearing capacity, the ductility and the ability of plastic redistribution of inner force of the TRC slab significantly. According to Chinese guideline (National Standard of the People's Republic of China, 2010), the allowable deflection of the slab is l/200 (l is the span length) in the serviceability stage, the load-bearing capacity of the

HSGTRC slab is higher than the RC slab even at the deflection of $l/100$ (corresponding to F_{100}), therefore, the hybrid use of the 50kg/m^3 steel fiber and AR glass fiber mesh is suitable for replacing of the conventional steel mesh with steel ratio of 0.2%.

One of the disadvantages of glass/basalt fiber mesh and TRC members without steel fibers is the brittleness and the poor energy absorption capacity after peak-load. The absorbed energy is an effective parameter to evaluate the effect of additional steel fibers as well as the hybrid effect of fiber mesh and steel fibers on the toughness of the two-way slab (Bernard, 2002;Cengiz and Turanli, 2004; Ding and Kusterle, 1999). The absorbed energy of different slabs is found by integrating the area under load-deflection curves, and can be calculated by Eqn.1 (European Federation of Producers and Applications of Specialist Products for Structures, 1996). The results of the energy absorption for different slabs can be seen in Table 6.

$$Q = \int_0^{\delta} F(x)dx \tag{1}$$

Where Q is the absorbed energy, J; δ is the central deflection of the slab, m; $F(x)$ is the force corresponding to x, N, respectively.

Table 6 Energy absorption of different slabs

Types	Energy absorption (J)			
	Q_{500}	Q_{250}	Q_{100}	Q_{50}
PC	15.9	—	—	—
BTRC	26.3	37.3	60.1	76.6
GTRC	27.8	53.3	71.7	84.3
RC	34.6	89.0	201.4	576.0
HSBTRC	41.3	108.6	324.8	578.4
HSGTRC	40.3	122.0	343.4	582.0

Note: Q_a (a=500, 250, 100, 50) means the energy absorption in the deflection from 0 to l/a, l is the span length.

Fig.14 shows the comparison of the energy absorption of BTRC slab, RC slab and HSBTRC slab.

Fig.14 Comparison of energy absorption of BTRC, RC and HSBTRC slabs

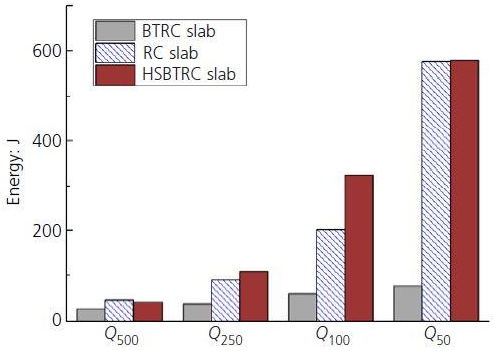

From Table 6 and Fig.14, it can be seen that:

i) When the deflection reaches to 2 mm, the Q_{250} of the RC slab, HSBTRC slab and HSGTRC slab are 89.0 J, 108.6 J and 122.0 J, respectively. Compared to the RC slab, the Q_{250} of HSBTRC slab and HSGTRC slab increase by about 22% and 37%, respectively.

ii) When the deflection reaches to 5 mm, the Q_{100} of the RC slab, HSBTRC slab and HSGTRC slab are 201.4 J, 324.8 J and 343.4 J, respectively. Compared to the RC slab, the Q_{100} of HSBTRC slab and HSGTRC slab increase by about 61% and 71%, respectively.

iii) When the deflection reaches to 10 mm, the Q_{50} of the RC slab, HSBTRC slab and HSGTRC slab are 576.0 J, 578.4 J and 582.0 J, respectively. Compared to the RC slab, the Q_{50} of HSBTRC slab and HSGTRC slab increase slightly (about 1%).

iv) The energy absorption up to a deflection of 10 mm of the HSBTRC and HSGTRC slabs are higher than that of the RC slab, as shown in Fig.14 for the comparison of the energy absorption of the RC and HSBTRC slab.

v) Based on the testing results and the ductile failure pattern, the conventional steel mesh can be replaced by the hybrid use of glass/basalt fiber mesh and 50 kg/m^{3}steel fibers.

The energy absorption capacity of the TRC slab with macro steel fibers is improved strongly. This behavior can be attributed to the reinforcement mechanism of macro steel fiber. After cracking, the fibers spanning across the cracks can transmit tensile loads, and a large amount of energy can be

absorbed in the process of de-bonding, slipping and pulling out of fibers (Cengiz and Turanli, 2004; Ding and Kusterle, 1999).

Fig.15 shows the comparison of the failure pattern and crack propagation at the bottom of the plain concrete slab and the basalt /glass fiber mesh reinforced concrete slab.

Fig.15 Failure patterns: (a) PC slab; (b) GTRC slab; (c) Broken down of the glass fiber

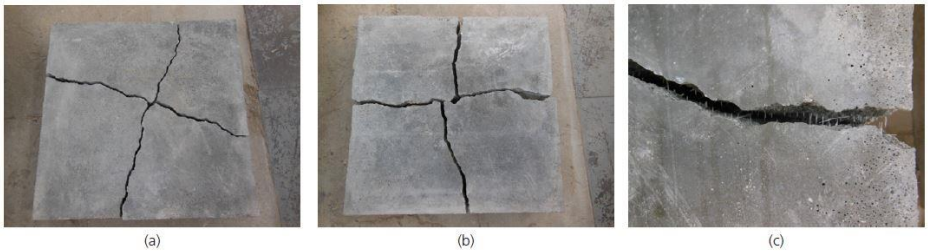

From Fig. 15 (a) and (b), it can be seen that the crack patterns of the PC slab and the fiber mesh reinforced concrete slab are similar. Due to the brittle properties of the basalt fiber and the AR glass fiber, the BTRC and GTRC slab still show clearly brittle behavior with small deflections. The fibers of the mesh across the cracks are mostly broken down, as shown in Fig.15 (c).

Fig.16 shows the comparison of the failure pattern and crack propagation of the RC slab and the TRC slab with hybrid reinforcement of fiber mesh and macro steel fiber (50kg/m^3).

Fig.16 Failure patterns: (a) RC slab; (b) HSBTRC slab

From Fig.16, it can be seen that:

i) Compared to the failure pattern of the TRC slabs without steel fiber in Fig.15(b), lots of cracks in the RC slab and TRC slab with steel fibers are formed, developed and radiate

outward to the edges from the centrally loaded zone. One of the important reasons is that the combined use of fiber mesh and macro steel fiber may show strong positive hybrid effect on the plastic redistribution ability of inner force and stress during the loading process.

ii) The crack widths are less and smaller than the slabs without steel fibers due mainly to the well distributed tensile stress.

iii) The failure mode of the BTRC/GTRC slab changes from brittle pattern into a ductile one. It means that the addition of the macro steel fiber aids in converting the brittle properties of the concrete into a ductile composite member.

4. Conclusions

Based on the experimental and analytical investigation, the following conclusions can be drawn:

1. The basalt fiber and AR glass fiber meshes demonstrate very good alkaline resistance and are selected to the further investigation on the mechanical property of TRC member.
2. For concrete with compressive strength about 51.0 MPa after 28d, compared to the PC slab, both the AR glass fiber mesh and basalt fiber mesh could enhance the bi-axial ultimate load of the two-way concrete slab by 49% and 58%, respectively, but the most brittle properties of the fiber mesh reinforced concrete remain unchanged.
3. Compared to the often used statically determinate beam or one-way panel test, the statically indeterminate two-way slab test is more suitable for investigation on the effect of fiber mesh on the bi-axial flexural property and ability of inner force redistribution of TRC slab.
4. The hybrid use of basalt/AR glass fiber mesh and macro steel fiber increase the loading bearing capacity and post-peak behavior as well as toughness of the TRC slab significantly. Compared to the BTRC slab, the energy absorption Q_{500}, Q_{250}, Q_{100}, Q_{50} of the HSBTRC slab increase by 57%, 191%, 440% and 655%, respectively.
5. The addition of macro steel fiber can change the brittle failure pattern of the BTRC and

GTRC slab into the ductile ones; enhance the residual load bearing capacity as well as the energy absorption capacity of the slab over the whole post-peak region strongly.

6. The load-deflection curves of HSBTRC slab and HSGTRC slab are higher than those of the RC slab over the deflection from 0-5 mm. The conventional steel mesh with constructive steel ration (0.2%) can be replaced by the hybrid use of basalt /AR glass fiber mesh and steel fibers with fiber content of 50 kg/m^3.

The present study provides a method to improve the ductility of the TRC member. Future study is needed to evaluate the hybrid effect of the fiber mesh with higher tensile strength and macro steel fiber with lower fiber dosage to replace the conventional steel mesh with higher reinforcement ratio.

Acknowledgements

The authors gratefully acknowledge the National Natural Science Foundation of China: Grants: 51578109 and 51421064.

References

Alhozaimy A M, Soroushian P and Mirza F (1996) Mechanical properties of polypropylene fiber reinforced concrete and the effects of pozzolanic materials. Cement and Concrete Composites, **18(2)**, 85-92.

Bernard E (2002) Correlations in the behaviour of fibre reinforced shotcrete beam and panel specimens. Materials & Structures, **35(3)**:156-164.

Bernat E, Gil L, Roca P and Escrig C (2013) Experimental and analytical study of TRM strengthened brickwork walls under eccentric compressive loading. Construction and Building Materials, **44**, 35-47.

Bentur A, Mindess S (2007) Fibre reinforced cementitious composites. Taylor & Francis.

Brameshuber W (2006) Textile reinforced concrete. State-of-the-art report of RILEM Technical Committee 201-TRC.

Cengiz O and Turanli L (2004) Comparative evaluation of steel mesh, steel fibre and high-performance polypropylene fibre reinforced shotcrete in panel test. Cement and Concrete Research, **34(8)**, 1357-1364.

Chira A, Kumar A, Vlach T, Laiblová L and Hajek P (2016) Textile-reinforced concrete facade panels with rigid foam core prisms. Journal of Sandwich Structures and Materials, **18(2)**, 200-214.

Ding Y, Liu H, Ning X, Zhang Y and Azevedo C (2014) Shear resistance and cracking behaviour of SFRC beams with and without axial load. Magazine of Concrete Research, **66(23)**, 1183-1193. http://dx.doi.org/10.1680/macr.14.00043.

Ding Y and Kusterle W (1999) Comparative study of steel fibre-reinforced concrete and steel mesh-reinforced concrete at early ages in panel tests. Cement and Concrete Research, **29(11)**, 1827-1834.

Enfedaque A, Cendón D, Gálvez F and Sánchez-Gálvez V (2010) Analysis of glass fiber reinforced cement (GRC) fracture surfaces. Construction and Building Materials, **24(7)**, 1302-1308.

European Federation of Producers and Applications of Specialist Products for Structures (1996). European specification for sprayed concrete, EFNARC. Loughborough: Loughborough University.

Friedrich M, Schulze A, Prösch G, Walter C, Weikert D, Binh N M and Zahn D R (2000) Investigation of chemically treated basalt and glass fibres. Microchimica Acta, **133(1-4)**: 171-174.

Gopinath S, Murthy AR, Iyer NR and Dharinee R (2016) Investigations on textile-reinforced concrete as cover for RC beams. Magazine of Concrete Research, **68(20)**: 1040-1050, http://dx.doi.org/10.1680/jmacr.15.00161.

Hou W, Zhang Z, Wang M, Li M and Sun Z (2007) Experimental study on acid and alkali resistance of basalt fiber used for composites. Acta Materiae Compositae Sinica, **24(6)**: 77-82. (in Chinese)

Jain K and Singh B (2013) Steel fibres as minimum shear reinforcement in reinforced concrete beams. Magazine of Concrete Research, **65(7)**: 430-440, https://doi.org/10.1680/macr.12.00113.

Larrinaga P, Chastre C, Biscaia H C and San-José J T (2014) Experimental and numerical modeling of basalt textile reinforced mortar behavior under uniaxial tensile stress. Materials and Design, **55**: 66-74.

Lee JH, Yoo DY, Yoon YS (2016) Mechanical behaviour of concrete with amorphous metallic and steel fibres. Magazine of Concrete Research, **68(24)**:1253-1264, http://dx.doi.org/10.1680/jmacr.15.00493.

Lim E, Vinayagam T, Wee T H and Thangayah T (2011) Shear transfer in fibre-reinforced lightweight concrete. Magazine of Concrete Research, **63(1)**: 13-20, https://doi.org/10.1680/macr.2011.63.1.13.

Li W and Xu J (2009) Mechanical properties of basalt fiber reinforced geopolymeric concrete under impact loading. Materials Science and Engineering: A, **505(1)**: 178-186.

Liu J, Jiang M, Wang Y, Wu G and Wu Z (2013) Tensile behaviors of ECR-glass and high strength glass fibers after NaOH treatment. Ceramics International, **39(8)**: 9173-9178.

Mehta P K, Monteiro P J M (2006) Concrete: microstructure, properties and materials. Prentice-Hall.

National Standard of the People's Republic of China (2010). Code for design of concrete structures. China Architecture and Building Press, Beijing, China.

Papanicolaou C G, Triantafillou T C, Karlos K and Papathanasiou M (2007) Textile-reinforced mortar (TRM) versus FRP as strengthening material of URM walls: in-plane cyclic loading. Materials and structures, **40(10)**: 1081-1097.

Purnell P, Short N R, Page C L and Majumdar A J (2000) Microstructural observations in new matrix glass fibre reinforced cement. Cement and Concrete Research, **30(11)**: 1747-1753.

Ros PS, Zerbino R, Martí-Vargas JR and Bossio, ME (2016) Creep and residual properties of cracked macro-synthetic fibre reinforced concretes. Magazine of Concrete Research, **68(4):** 1-11, http://dx.doi.org/10.1680/macr.15.00111.

Rybin V A, Utkin A V and Baklanova N I (2013) Alkali resistance, microstructural and mechanical performance of zirconia-coated basalt fibers. Cement and Concrete Research, **53**: 1-8.

Scheffler C, Förster T, Mäder E, Heinrich G, Hempel S and Mechtcherine V (2009) Aging of alkali-resistant glass and basalt fibers in alkaline solutions: Evaluation of the failure stress by Weibull distribution function. Journal of Non-Crystalline Solids, **355(52)**: 2588-2595.

Shams A, Hegger J and Horstmann M (2014a) An analytical model for sandwich panels made of textile-reinforced concrete. Construction and Building Materials, **64:** 451-459.

Shams A, Horstmann M and Hegger J (2014b) Experimental investigations on textile-reinforced concrete (TRC) sandwich sections. Composite Structures, **118:** 643-653.

Sim J, Park C and Moon D Y (2005) Characteristics of basalt fiber as a strengthening material for concrete structures. Composites Part B Engineering, **36(6–7)**: 504-512.

Singh H (2016) Strength and performance of steel fibre-reinforced concrete stiffened plates. Magazine of Concrete Research, **68(5)**: 250-259, http://dx.doi.org/10.1680/jmacr.15.00043.

Song P S, Hwang S and Sheu B C (2004) Statistical evaluation for impact resistance of steel-fibre-reinforced concretes. Magazine of Concrete Research, **56(8)**: 437-442, https://doi.org/10.1680/macr.2004.56.8.437.

Triantafillou T C and Papanicolaou C G (2006) Shear strengthening of reinforced concrete members with textile reinforced mortar (TRM) jackets. Materials and structures, **39(1)**: 93-103.

Wang L, Wang H and Jia J (2009) Impact resistance of steel-fibre-reinforced lightweight-aggregate concrete. Magazine of Concrete Research, **61(7)**: 539-547. https://doi.org/10.1680/macr.2007.00128.

Wei B, Cao H and Song S (2010) Tensile behavior contrast of basalt and glass fibers after chemical treatment. Materials and Design, **31(9)**: 4244-4250.

You ZG, Wang XG, Liu GH, Chen HB and Li SX (2017) Shear behaviour of hybrid fibre-reinforced SCC T-beams. Magazine of Concrete Research, **69(18)**: 919-938, http://dx.doi.org/10.1680/jmacr.16.00470

Zollo R F (1997) Fiber-reinforced concrete: an overview after 30 years of development. Cement and Concrete Composites, **19(2)**: 107-122.

Zargaran M, Attari N K, Alizadeh S and Teymouri P (2017) Minimum reinforcement ratio in TRC panels for deflection hardening flexural performance. Construction and Building Materials, **137**: 459-469.